Unraveling the Diffusion Properties of Zeolite-Based Multicomponent Catalyst by Combined Gravimetric Analysis and IR Spectroscopy (AGIR)

Peng Peng, Dusan Stosic, Abdelhafid Aitblal, Alexandre Vimont, Philippe Bazin, Xin-Mei Liu, Zi-Feng Yan, Svetlana Mintova, Arnaud Travert

Unraveling the diffusion properties of zeolite-based multi-component catalyst by combined Gravimetric Analysis and IR spectroscopy (AGIR)

Peng Peng[†,‡], Dusan Stosic[‡], Abdelhafid A. Blal[‡], Alexandre Vimont[‡], Philippe Bazin[‡], Xin-Mei Liu[†], Zi-Feng Yan[†], Svetlana Mintova[†,‡]*, & Arnaud Travert[‡]**

[†]State Key Laboratory of Heavy Oil Processing, China University of Petroleum, Qingdao 266580, China

[‡]Laboratoire Catalyse et Spectrochimie (LCS), Normandie Univ, ENSICAEN, UNICAEN, CNRS, 14000 Caen, France

KEYWORDS model zeolite-based catalyst, internal diffusion, catalyst effectiveness factor, hierarchical zeolite, *operando* analysis, combined gravimetric and infrared spectroscopy analysis Gravimetric Analysis and IR spectroscopy (AGIR)

ABSTRACT Concept of pore hierarchization for enhancing zeolite catalytic performance has been the main focus during the last decade; the main research activities widely emphasized on the preparation of single-component hierarchical zeolite catalysts. Here we report on the critical aspect of interconnectivity of multi-components in hierarchical zeolite catalysts using an *operando* combined gravimetric and infrared spectroscopy (AGIR) analyses. The variances of macroscopic diffusion behaviors between the global multi-component catalyst (indexed as global diffusion time constant) and its zeolitic moiety (indexed as micropore diffusion time constant) are differentiated via simultaneous gravimetric and infrared analysis, respectively. The effectiveness factors correlated with the diffusion time constants show that the non-ideal interconnectivity between the zeolitic and non-zeolitic components weakens the full potential of the multi-component catalyst.

1. Introduction

Zeolite-based catalysts have been successfully used in many catalytic processes such as energy conversion, chemical fabrication, environmental catalysis, *etc*[1]. However, the intrinsic microporosity of zeolites often leads to intracrystalline diffusion limitations when molecules with kinetic diameters larger than the pore size of zeolites are processed[2]. The concept of pore hierarchization, based on the introduction of mesopores into zeolites to improve internal diffusion properties has received much attention during the last decades[3–5]. Numerous studies have demonstrated substantial beneficial effects on alleviating diffusion limitations of hierarchical zeolitic materials[6,7]. Hierarchical zeolites also showed superior performances in many hydrocarbon conversion reactions such as catalytic cracking[8], methanol-to-hydrocarbons[9–11], alkylation[12,13], aldol condensation[14,15], esterification[16], or hydrogenation[17,18].

Despite the promising progresses in the synthesis of hierarchical zeolitic materials, a question of urgent relevance is to quantitatively assess and correlate the actual diffusion properties of hierarchical zeolites used for the preparation of actual industrial catalysts. Different from single-component hierarchical zeolite catalysts used at the laboratory scale, real industrial catalysts (pre-shaped bodies) contain many non-zeolitic components like silica, alumina, amorphous aluminosilicate or clays to guarantee their mechanical strength, hydrothermal stability, and resistance to poisoning[19,20]. The introduction of such non-zeolitic components can unavoidably result in changes of catalytic performances of the catalyst bodies[21,22]. While the diffusion and pore interconnection properties of the single-component hierarchical zeolites synthesized by various methods have been intensively studied[23–25], reports on the diffusivity measurements of hierarchical zeolites in an environment of multi-component catalyst are still scarce. One of the difficulties behind is that classical macroscopic measurements of diffusion (*e.g.* sole volumetric or gravimetric

methods) only yields the global effective diffusivity in the multi-component (industrial) catalyst[26]. Such methods cannot directly indicate whether the guest adsorbate molecules have a faster or slower access to the corresponding active sites, which are mostly located in zeolitic components of the multi-component catalyst[27]. Alternatively, pulsed field gradient nuclear magnetic resonance (PFG NMR) is used to evaluate the interconnectivity between microporous and mesoporous structures[28,29]. However, in order to understand the diffusivity in the microporous network of zeolitic component from the measured effective diffusivity, a combination of rules and various phenomenological models have to be relied on for the interpretation of PFG NMR data[26]. Therefore, a new analytical *operando* characterization technique able to differentiate the macroscopic diffusion behaviour of zeolitic component from multi-component catalyst, is being highly looked forward.

In this paper, we report the macroscopic diffusion properties of 2,2,4-trimethylpentane (isooctane) in parent single-component ZSM-5 catalyst (ZSM-5-P), hierarchical single-component ZSM-5 catalyst (ZSM-5-A) and model multi-component zeolite-based catalyst (ZSM-5-AR) by simultaneous use of *operando* gravimetric and infrared spectroscopy analyses (AGIR). Isooctane was chosen as a probe molecule due to its kinetic diameter (0.62 nm)[30,31] that is larger than pore openings of the ZSM-5 zeolite (0.55 nm)[32–35]. A model multi-component zeolite-based catalyst was prepared by sequential alkali dissolution of a commercial ZSM-5 followed by MCM-41 like mesostructure re-assembly (denoted as ZSM-5-AR). The diffusivity and catalytic properties of the multi-component zeolite-based catalyst ZSM-5-AR were compared with the parent ZSM-5 zeolite (ZSM-5-P) and its alkali treated counterpart (ZSM-5-A). In the ZSM-5-AR, MCM-41 mesostructure, which are *per se* amorphous aluminosilicate is generated under the treatment with cetyl trimethyl ammonium bromide (CTAB)[36]; the MCM-41 is usually overgrown on the surface

of alkali-dissolved zeolite crystal phase[8,37,38]. This intimate contact between the two phases makes the mesostructured materials significantly different from a mechanical mixture of a hierarchical zeolite phase and an ordered mesostructure phase[6]; this material mimics the change of pore structure during the shaping of industrial catalyst. Details of the synthesis, textural and acid properties of the samples are presented in Supplementary Information (SI), Figures S1-S5 and Tables S1-S2. Quantitative correlations between the measured macroscopic diffusion properties of the zeolitic component from the catalyst (parent single-component ZSM-5 catalyst, hierarchical single-component ZSM-5 catalyst and model multi-component zeolite-based catalyst) and their catalyst effectiveness correlated via Thiele modulus were also established.

2. Experimental

2.1 Combined gravimetric analysis and infrared spectroscopy (AGIR)

The three samples were tested by AGIR using isooctane as probe adsorbate. A SETARAM SETSYS-B microbalance with sensitivity of 0.1 μg was adopted for microbalance data acquisition, while Thermo Nicolet 6700 Fourier transform infrared spectrometer was used for IR data acquisition. Detailed information on AGIR apparatus can be found in ref. 32. All the samples were pressed into self-supporting wafers (diameter: 1.6 cm, mass: 20 mg) and activated at 723 K under a flow of argon of 25 mL min^{-1} for 6 hours and then maintained under the flow of argon at 423 K. Then isooctane was fed from a saturator at 293 K into the cell of AGIR under argon at 423 K. The isooctane pressure was estimated by Antoine Equation and the related parameters were available from National Institute of Standards and Technology of America (NIST).

The quantification of the diffusion properties was derived from the following relationship, which is valid for the initial uptake for particles of arbitrary shapes assuming that the internal diffusion is rate controlling:[26]

$$\frac{q(t)}{q(\infty)} \approx \frac{2}{\sqrt{\pi}}\left(\frac{D_{eff}}{L^2}t\right)^{\frac{1}{2}} = \frac{2}{\sqrt{\pi}}\left(\frac{t}{\tau}\right)^{\frac{1}{2}} \quad (1)$$

where $q(t)$ and $q(\infty)$ are the uptake of isooctane at time t and at equilibrium, respectively, D_{eff} is the effective diffusivity, and L is an effective diffusion path length defined as the ratio of external surface area to particle volume. The characteristic diffusion time constant $\tau^{-1} = D_{eff}/L^2$ can be obtained from the slope of linear portion of the fractional uptake versus square root of time plots.

Based on the gravimetric and IR spectroscopy analysis, two fractional uptakes ($q(t)/q(\infty)$) were expressed as the following: (1) the global fractional uptake based on gravimetric analysis and (2) the BAS fractional coverage based on infrared spectroscopy analysis, from which two characteristic diffusion time constants were derived: τ_{global}^{-1} and τ_{OH}^{-1}, respectively.

2.2 Reaction conditions for isooctane cracking

The three samples (granules with diameter of 200-400 μm) were tested in isooctane cracking reaction conducted at atmospheric pressure in a fixed bed reactor (10 mm internal diameter). Prior to the reaction, the samples were purged under a flow of air at 723 K for 4 hours. Afterwards, isooctane was fed into the reactor with nitrogen as carrier gas at the same temperature. The reactant and products were on-line analyzed by a Varian CP 3900 gas chromatograph equipped with a 25 m × 0.25 mm × 0.25 μm HP-PONA capillary column and a flame ionization detector. Considering that the isooctane conversion of ZSM-5-A is higher than 10 %, the observed reaction rates were calculated based on the integrated equation[39,40]:

$$r_0 = \frac{F}{W}\ln\frac{1}{1-X_0} \quad (2)$$

Where r_o is the observed initial reaction rate of isooctane cracking, F is the molar flow rate of isooctane, W is the weight of the catalyst. In this study, F and W were fixed to 0.105 mmol min^{-1}

and 40 mg, respectively. X_0 is the initial conversion of isooctane, which was measured at 3 min after the commencement of the reaction.

3. Results and Discussion

3.1 Diffusion of isooctane in zeolite based catalysts studied by *operando* AGIR

The isooctane uptake curves for all samples as determined by gravimetric analysis are depicted in Figure 1. The uptakes at equilibrium on samples ZSM-5-A and ZSM-5-AR are quite close and lower than that of the parent zeolite (ZSM-5-P). This is in agreement with the reduction of micropore volume and Brønsted acid sites (BAS) amount measured by infrared (IR) using a pyridine as a probe molecule (Figure S3 and Table S2). However, at the initial stage of the diffusion process, the apparent diffusion rate of isooctane in the ZSM-5-P is lower than that of the hierarchical samples (Figure 1B). Linear relationship between normalized global fractional uptake of isooctane and the square root of diffusion time obtained from the microbalance of all samples are depicted in Figure 1C. D_{eff} is typically calculated by assuming spherical particles so that L is one third of particle radius. However, as shown in the work of Vattipalli *et al.*[41], the apparent diffusion lengths determined for hierarchical porous materials are significantly longer than those predicted by the physical structure (*i.e.*, radius) of the adsorbent, indicating that diffusion of molecules in such structures is much longer than expected. Inappropriate estimation of this parameter can further cause errors in estimation of diffusivity. For these reasons, we have not attempted to derive the effective diffusivities D_{eff}, and only considered the value of the *global* diffusion time constant $\tau_{global}^{-1} = D_{eff}/L^2$ derived from the slope of the fractional uptake versus $t^{\frac{1}{2}}$ curves; the values obtained for the three samples are summarized in Table 1. The enhancement of two orders of magnitude of τ_{global}^{-1} for hierarchical ZSM-5-A and ZSM-5-AR in comparison to parent ZSM-5-P sample is revealing the large increase of the isooctane diffusion rate in former

samples. These results are in a good accordance with the work of Groen *et al.*[42] and Pérez-Ramírez *et al.*,[13] unambiguously showing the primary consequence of introducing mesopores into microporous (zeolite) structures in term of diffusion rate in the catalyst particles.

The accessibility of acidic active sites of zeolite in a multi-component catalyst is governed by the location and distribution of bridged hydroxyl groups (Si-O(H)-Al); stretching vibrations at *c.a.* 3610 cm^{-1} in the IR spectra is indicating their presence[43]. Consistent with the results based on pyridine and collidine adsorption (Figures S3-S5), the BAS of all samples are located in the micropores of zeolite phase and thus consist of framework bridged hydroxyl groups (Si-O(H)-Al), which also can be observed as stretching vibrations at *c.a.* 3610 cm^{-1} (Figure S6).

Therefore, direct quantitative measurements of the diffusion towards the micropores of zeolite can be performed based on the coverage of Si-O(H)-Al as a function of time (Figure 2A, B, Figure S7). A linear relationship is obtained plotting the normalized relative coverage of Si-O(H)-Al versus the square root of time (Figure 2C). The corresponding *micropore* diffusion time constant, which is indexed as τ_{OH}^{-1}, is summarized in Table 1. Comparison of this parameter for the three samples show an enhancement of the rate of diffusion towards the micropores for sample ZSM-5-A and in a lesser extent for ZSM-5-AR with respect to the parent sample ZSM-5-P.

Comparison of τ_{global}^{-1} and τ_{OH}^{-1} for all samples show that they present close values for samples ZSM-5-P and ZSM-5-A. This indicates that the overall improvement of diffusion brought by the mesoporosity of sample ZSM-5-A improves *in the same extent* the diffusion towards the BAS sites located in the micropores[13,42]. This strongly reveals the good interconnectivity between meso- and micro- porous networks in sample ZSM-5-A made via alkali dissolution[10]. In contrast, τ_{OH}^{-1} for sample ZSM-5-AR is one order of magnitude lower than τ_{global}^{-1} determined from the gravimetric analysis, with a difference far beyond the error of experimental measurements. Hence, while the

presence of the non-zeolitic component (MCM-41 like mesostructure) does enhance the overall rate of diffusion of isooctane in the ZSM-5-AR more than in ZSM-5-P, it leads to a significant decrease of the diffusion rate towards the BAS of ZSM-5-AR with respect to the single-component counterpart (ZSM-5-A). As mentioned above, bulky probe molecules like isooctane cannot directly interact with BAS within the zeolite pores. Instead, they have to adsorb firstly on the external surface and then transport from the surface to the BAS via micropore diffusion. Therefore, τ_{OH}^{-1} is related to the diffusion towards and within the micropores, while τ_{global}^{-1} only reflects the rate of uptake by the catalyst.

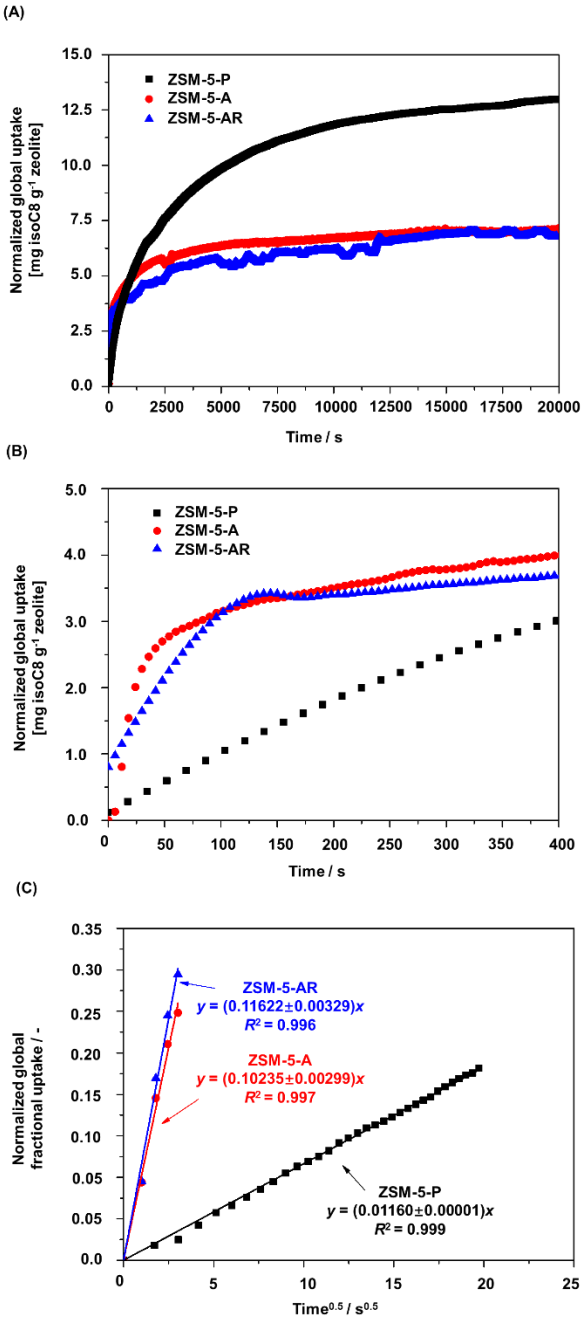

Figure 1. Isooctane uptake curves for parent ZSM-5 catalyst (ZSM-5-P), hierarchical single-component ZSM-5 catalyst (ZSM-5-A) and multi-component zeolite-based catalyst (ZSM-5-AR) measured by microbalance using operando AGIR: normalized global uptake in the whole range of time (20000 sec) (A), normalized global uptake in a short range of time (400 sec) (B), and normalized global fractional uptake as square root of time (C).

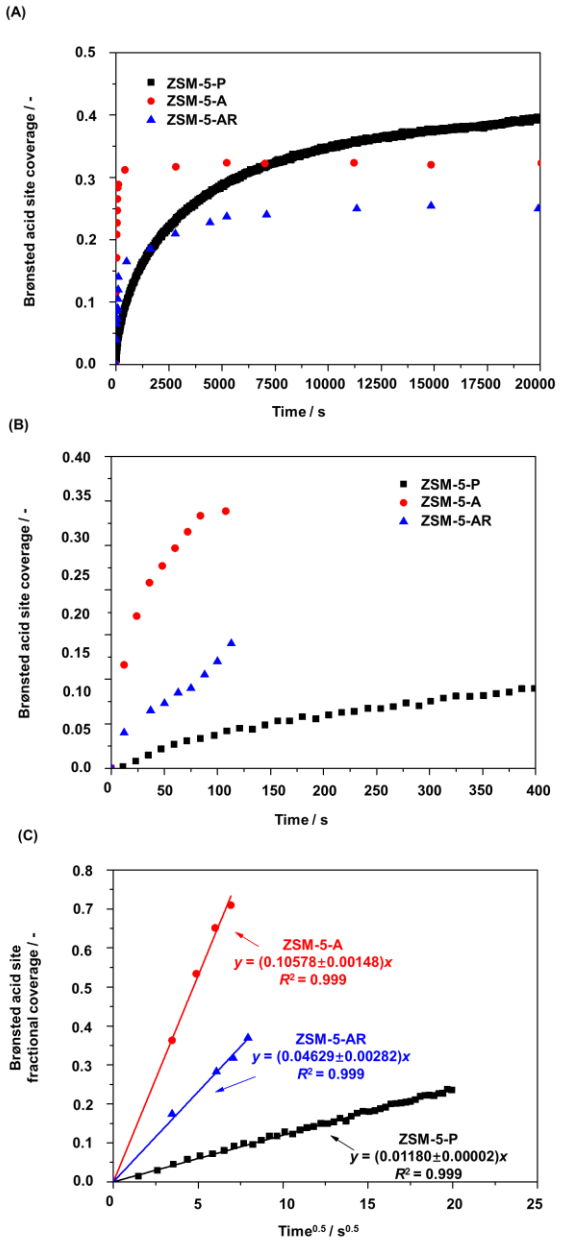

Figure 2. Isooctane uptake curves of parent single-component ZSM-5 catalyst (ZSM-5-P), hierarchical single-component ZSM-5 catalyst (ZSM-5-A) and multi-component zeolite-based catalyst (ZSM-5-AR) measured by IR using operando AGIR technique: (A) Brønsted acid site coverage in the whole time range (20000 sec), (B) Brønsted acid site coverage in a short time range (400 sec), and (C) Brønsted acid site fractional coverage as square root of time.

The deviation of the diffusion time constants for ZSM-5-AR sample can be interpreted in terms of undesired interconnectivity between the zeolitic and non-zeolitic components. In the case of ZSM-5-A, which is the single-component ZSM-5 based catalyst, its mesopores are traced back to the voids due to the removal of aluminosilicate species from zeolite crystals. Since the resulting voids originate from the zeolite framework, they are inherently connected to intracrystalline micropores and zeolite active sites (Figure 3B, E). On the contrary, the non-zeolitic ordered mesostructures in sample ZSM-5-AR are formed via overgrowth of alkali dissolved aluminosilicate species on the surface of single-component hierarchical ZSM-5 catalyst (*i.e*. ZSM-5-A). As shown in the TEM image of ZSM-5-AR (Figure 3C), the direction and orientation of such non-zeolitic mesopores appear randomly distributed (Figure 3F). Therefore, there is no reason why such mesoporous structures should be well-connected with the zeolitic micropores and thus lead to the blockage or narrowing of the access to them. Furthermore, while the overall improvement of the global rate of uptake brought by mesoporosity is similar for ZSM-5-A and ZSM-5-AR (Figure 1), the improvement is much less for ZSM-5-AR when considering the rate of uptake measured based on OH groups (Figure 2). In this sense, the divergence between τ_{global}^{-1} and τ_{OH}^{-1} for ZSM-5-AR sample is a clear indication for undesired interconnection between micro- and mesoporous networks within the model catalyst. Here the *operando* AGIR technique can simultaneously determine the macroscopic diffusion rates of the global catalyst and the framework OH groups located at the zeolitic component, thus revealing it as an efficient analytical tool for pore interconnectivity in multi-component catalyst.

Table 1. Diffusion time constants of parent single-component ZSM-5 catalyst (ZSM-5-P), hierarchical single-component ZSM-5 catalyst (ZSM-5-A) and multi-component zeolite-based catalyst (ZSM-5-AR) calculated from the microbalance (τ_{global}^{-1}) and IR data (τ_{OH}^{-1}) using AGIR technique.

Sample	τ_{global}^{-1} **[10^4/s^{-1}]**	τ_{OH}^{-1} **[10^4/s^{-1}]**
ZSM-5-P	(1.1±0.0)	(1.1±0.0)
ZSM-5-A	(82.3±4.0)	(87.8±2.5)
ZSM-5-AR	(106.1±5.8)	(16.8±1.8)

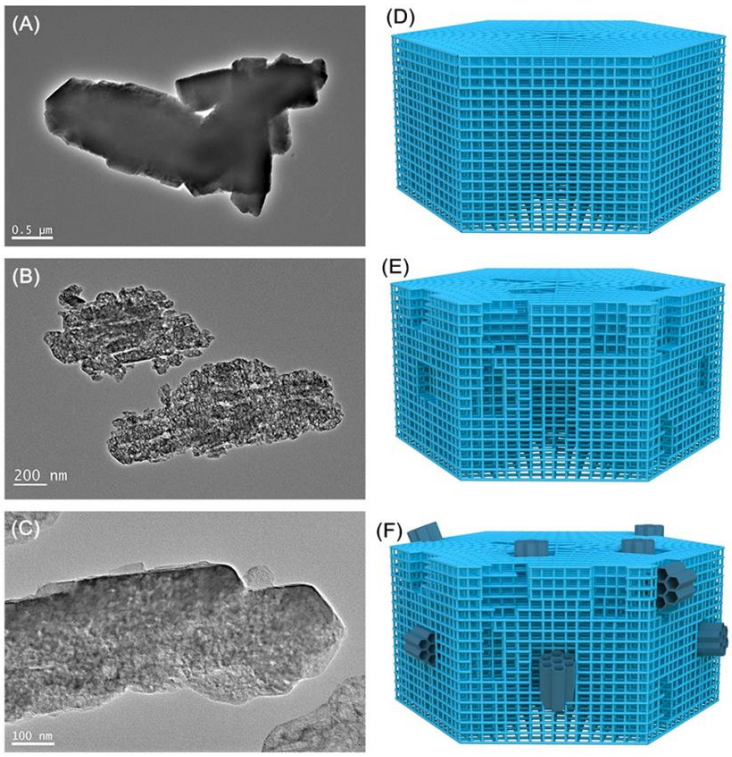

Figure 3. TEM images and schematic diagrams of parent single-component ZSM-5 catalyst (ZSM-5-P) (A, D), hierarchical single-component ZSM-5 catalyst (ZSM-5-A) (B, E) and multi-component zeolite-based catalyst (ZSM-5-AR) (C, F)

3.2 Assessment of catalyst effectiveness factor of the zeolite based catalysts in isooctane cracking

The performances of the catalysts in isooctane cracking were assessed; the pore blocking or narrowing were quantitatively evaluated and their impact on the catalytic properties was determined. As shown in Figure 4, the initial conversions of the three samples are found to vary by a factor of 3, and the conversions gradually decrease due to coke accumulation[44] (Figure 4A). As a typical cracking reaction that is widely used in petroleum refinery industry, the contemporary fluid catalytic cracking (FCC) processes is normally carried out in riser reactors, where the contact time of the feedstock with the FCC catalyst is very short[45].

Further the discussion will be focused on the cracking behaviour of the samples in the beginning of the reaction. The initial cracking rate constants are 0.369, 0.232 and 0.110 mmol g^{-1} min^{-1} for samples ZSM-5-A, ZSM-5-AR and ZSM-5-P, respectively (Figure 4B). It is worth mentioning that ZSM-5-A and ZSM-5-AR present lower numbers of BAS with respect to the parent zeolite sample, but higher observed reaction rates, suggesting that increased accessibility of BAS ameliorate the performance of the zeolites. Further, the initial rate constants are clearly correlated to τ_{OH}^{-1}, *rather than* to τ_{global}^{-1}, even after correcting the differences of acid site concentrations (*vide infra*). This further validates the interest in monitoring the framework OH groups by *operando* AGIR.

The internal diffusion of zeolite based catalysts using *operando* AGIR was utilized to assess the catalyst effectiveness factor in isooctane cracking. The calculation protocol applied is presented in the SI. The plot representing the catalysts effectiveness factor versus Thiele modulus with highlighting the value for the three catalysts in the current study is shown in Figure 5. The catalyst effectiveness factor of the hierarchical samples, ZSM-5-A (0.86-0.93) and ZSM-5-AR (0.72-0.84),

are much higher than for the parent zeolite (0.07-0.11), confirming that the introduction of hierarchical zeolitic component decrease the inherent diffusion limitations of the microporous channels.

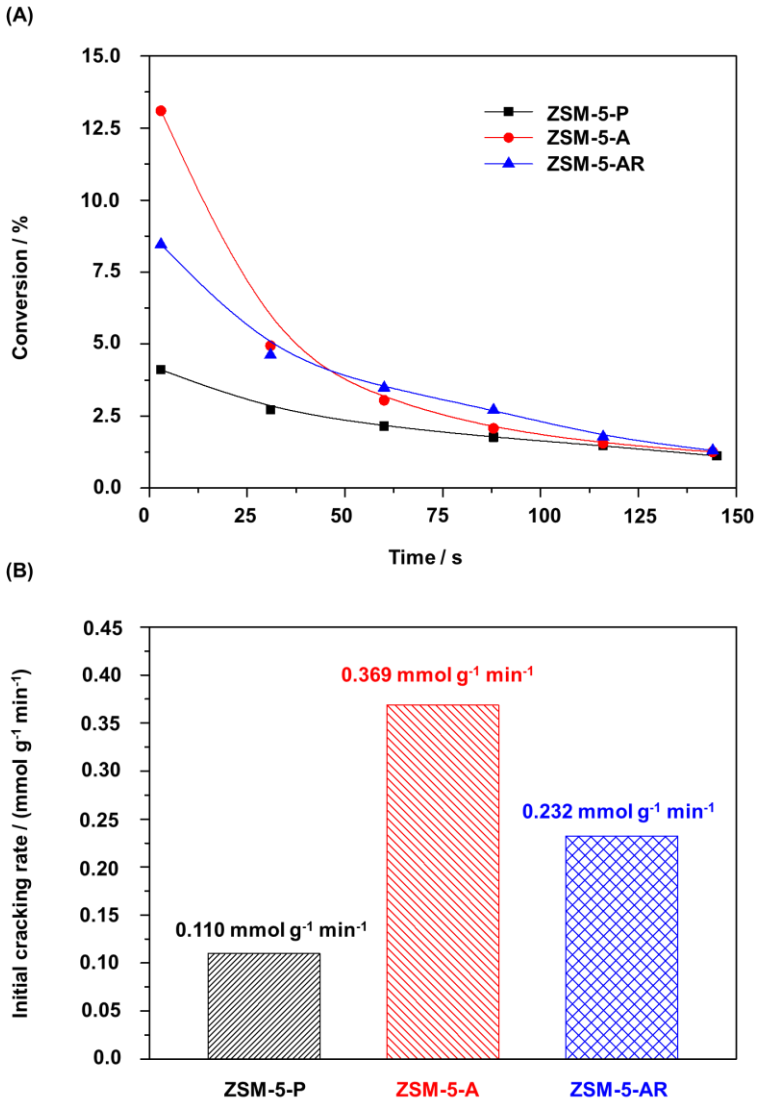

Figure 4. Isooctane cracking conversion as a function of time on stream (A) and initial cracking rates (B) for parent single-component ZSM-5 catalyst (ZSM-5-P), hierarchical single-component ZSM-5 catalyst (ZSM-5-A) and multi-component zeolite-based catalyst (ZSM-5-AR)

However, the lower efficiency of ZSM-5-AR compared with that of ZSM-5-A confirms that non-ideal pore interconnection between zeolitic and non-zeolitic ingredients of the model multi-component zeolite-based catalyst body may prevent the full utilization of zeolite crystals in catalytic cracking of isooctane. Therefore, industrial exploitation of hierarchical zeolites should not only focus on the rational structural design of hierarchical zeolitic materials themselves, but also pay more attention on the pore connectivity between zeolitic and non-zeolitic components within multi-component catalyst.

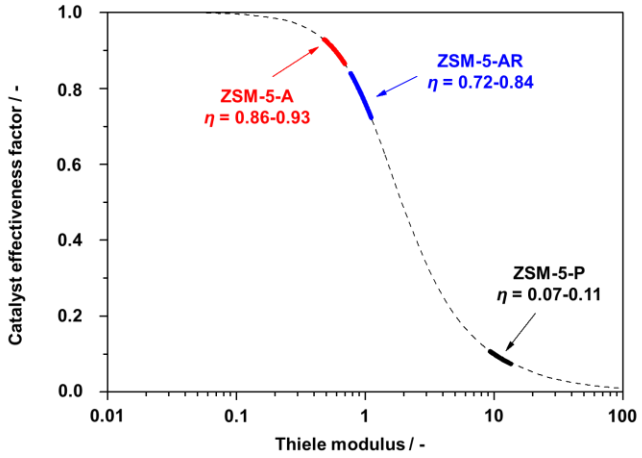

Figure 5. Estimated catalyst effectiveness factors (η) of parent ZSM-5 catalyst (ZSM-5-P), hierarchical single-component ZSM-5 catalyst (ZSM-5-A) and multi-component zeolite-based catalyst (ZSM-5-AR) in isooctane cracking.

Conclusion

In summary, combined gravimetric and IR spectroscopy analysis (AGIR) was used to study the diffusion properties of a zeolite-based multi-component catalyst consisting of meso- and micro-porous components and compared to hierarchical single-component ZSM-5 catalyst (ZSM-5-A) and multi-component zeolite-based catalyst (ZSM-5-AR). The kinetics of isooctane uptake on the catalyst and on Brønsted acid sites were determined. The corresponding characteristic diffusion

times were consistent for both single-component catalysts, indicating in particular a good interconnectivity between meso- and micro- porous networks. In contrast, for the model multi-component zeolitic catalyst (ZSM-5-AR), the deviation of characteristic diffusion time constants obtained from the global fractional uptake (τ_{global}^{-1}) and the BAS fractional coverage (τ_{OH}^{-1}) indicate the non-ideal interconnectivity between the zeolitic and non-zeolitic components. This conclusion was confirmed by comparing the catalysts performance in isooctane cracking and assessing the Thiele moduli and catalysts effectiveness of zeolite based materials. The interplay between zeolitic and non-zeolitic components may be detrimental and decrease the potential of a single-component hierarchical catalyst. Hence, more attention on the pore connectivity between zeolitic and non-zeolitic components should be paid for the development of efficient multicomponent catalysts. Finally, monitoring the uptake kinetics of zeolite acid sites by *operando* spectroscopy can be considered as a promising analytical tool of zeolite-based multicomponent catalysts.

AUTHOR INFORMATION

Corresponding Author

*Zi-Feng Yan: zfyancat@upc.edu.cn

*Svetlana Mintova: svetlana.mintova@ensicaen.fr

*Arnaud Travert: arnaud.travert@ensicaen.fr

Funding Sources

This work was funded from Chinese Scholarship Council (CSC), K. C. Wong Education Foundation, Thousand Talents Program for Foreign Experts (WQ20152100284), Key Projects of China National Key R&D Plan (2018YFE0118200), Key Projects of Shandong Provincial Key

R&D Plan (2019JZZY010506), and Major Projects of PetroChina on Catalysts of Oil Processing (No. 2016E-0707).

ACKNOWLEDGMENT

The authors acknowledge Dr. Huai-Ping Wang and Dr. Yan-Peng Li from China University of Petroleum for their help and contributions on XRD and TEM measurements, respectively.

TABLE OF CONTENT

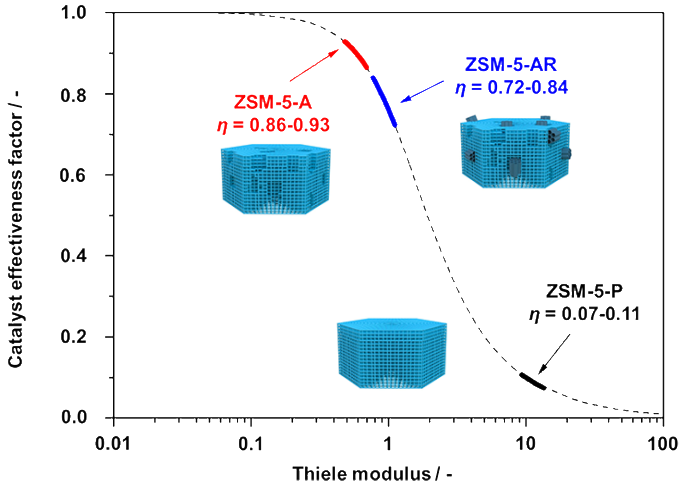

REFERENCES

(1) Martínez, C.; Corma, A. Inorganic Molecular Sieves: Preparation, Modification and Industrial Application in Catalytic Processes. *Coord. Chem. Rev.* **2011**, *255* (13–14), 1558–1580.

(2) Spangsberg, M.; Taarning, E.; Egeblad, K.; Hviid, C. Catalysis with Hierarchical Zeolites. *Catal. Today* **2011**, *168* (1), 3–16.

(3) Masoumifard, N.; Guillet-Nicolas, R.; Kleitz, F. Synthesis of Engineered Zeolitic Materials: From Classical Zeolites to Hierarchical Core–Shell Materials. *Adv. Mater.* **2018**, *30* (16), 1704439.

(4) Valtchev, V.; Mintova, S. Hierarchical Zeolites. *MRS Bull.* **2016**, *41* (9), 689–693.

(5) Möller, K.; Bein, T. Mesoporosity-a New Dimension for Zeolites. *Chem. Soc. Rev.* **2013**, *42* (9), 3689–3707.

(6) Galarneau, A.; Guenneau, F.; Gedeon, A.; Mereib, D.; Rodriguez, J.; Fajula, F.; Coasne, B. Probing Interconnectivity in Hierarchical Microporous/Mesoporous Materials Using Adsorption and Nuclear Magnetic Resonance Diffusion. *J. Phys. Chem. C* **2016**, *120* (3), 1562–1569.

(7) Zhou, J.; Liu, Z.; Wang, Y.; Gao, H.; Li, L.; Yang, W.; Xie, Z.; Tang, Y. Enhanced Accessibility and Utilization Efficiency of Acid Sites in Hierarchical MFI Zeolite Catalyst for Effective Diffusivity Improvement. *RSC Adv.* **2014**, *4* (82), 43752–43755.

(8) Peng, P.; Wang, Y.; Rood, M. J.; Zhang, Z.; Subhan, F.; Yan, Z.; Qin, L.; Zhang, Z.; Zhang, Z.; Gao, X. Effects of Dissolution Alkalinity and Self-Assembly on ZSM-5-Based Micro-/Mesoporous Composites: A Study of the Relationship between Porosity, Acidity, and Catalytic Performance. *CrystEngComm* **2015**, *17* (20), 3820–3828.

(9) Tian, Q.; Liu, Z.; Zhu, Y.; Dong, X.; Saih, Y.; Basset, J.-M.; Sun, M.; Xu, W.; Zhu, L.; Zhang, D.; et al. Beyond Creation of Mesoporosity: The Advantages of Polymer-Based Dual-Function Templates for Fabricating Hierarchical Zeolites. *Adv. Funct. Mater.* **2016**, *26* (12), 1881–1891.

(10) Milina, M.; Mitchell, S.; Crivelli, P.; Cooke, D.; Pérez-Ramírez, J. Mesopore Quality Determines the Lifetime of Hierarchically Structured Zeolite Catalysts. *Nat. Commun.* **2014**, *5*, 3922.

(11) Tang, Q.; Xu, H.; Zheng, Y.; Wang, J.; Li, H.; Zhang, J. Catalytic Dehydration of Methanol to Dimethyl Ether over Micro-Mesoporous ZSM-5/MCM-41 Composite Molecular Sieves. *Appl. Catal. A Gen.* **2012**, *413–414*, 36–42.

(12) Liu, H.; Xie, S.; Xin, W.; Liu, S.; Xu, L. Hierarchical ZSM-11 Zeolite Prepared by Alkaline Treatment with Mixed Solution of NaOH and CTAB: Characterization and Application for Alkylation of Benzene with Dimethyl Ether. *Catal. Sci. Technol.* **2016**, *6* (5), 1328–1342.

(13) Peréz-Ramírez, J.; Verboekend, D.; Bonilla, A.; Abelló, S. Zeolite Catalysts with Tunable Hierarchy Factor by Pore-Growth Moderators. *Adv. Funct. Mater.* **2009**, *19* (24), 3972–3979.

(14) Du, X.; Yang, Y.; Shi, D.; Lin, C.; Qiu, Y.; Sun, J. The Construction of a Series of Hierarchical MWW-Type Zeolites and Their Catalytic Performances for Bulky Aldol Condensation. *Microporous Mesoporous Mater.* **2018**, *268*, 117–124.

(15) Choi, M.; Cho, H. S.; Srivastava, R.; Venkatesan, C.; Choi, D.-H.; Ryoo, R. Amphiphilic Organosilane-Directed Synthesis of Crystalline Zeolite with Tunable Mesoporosity. *Nat. Mater. Mater* **2006**, *5* (9), 718–723.

(16) Srivastava, R.; Choi, M.; Ryoo, R. Mesoporous Materials with Zeolite Framework: Remarkable Effect of the Hierarchical Structure for Retardation of Catalyst Deactivation. *Chem. Commun.* **2006**, No. 43, 4489–4491.

(17) Gu, J.; Zhang, Z.; Hu, P.; Ding, L.; Xue, N.; Peng, L.; Guo, X.; Lin, M.; Ding, W. Platinum Nanoparticles Encapsulated in MFI Zeolite Crystals by a Two-Step Dry Gel Conversion Method as a Highly Selective Hydrogenation Catalyst. *ACS Catal.* **2015**, *5* (11), 6893–6901.

(18) Sun, Y.; Prins, R. Hydrodesulfurization of 4,6-Dimethyldibenzothiophene over Noble Metals Supported on Mesoporous Zeolites. *Angew. Chem. Int. Ed.* **2008**, *47* (44), 8478–8481.

(19) Mitchell, S.; Michels, N.-L.; Pérez-Ramírez, J. From Powder to Technical Body: The Undervalued Science of Catalyst Scale Up. *Chem. Soc. Rev.* **2013**, *42* (14), 6094–6112.

(20) Gueudré, L.; Milina, M.; Mitchell, S.; Pérez-Ramírez, J. Superior Mass Transfer Properties of Technical Zeolite Bodies with Hierarchical Porosity. *Adv. Funct. Mater.* **2014**, *24* (2), 209–219.

(21) Hosseinpour, N.; Mortazavi, Y.; Bazyari, A.; Khodadadi, A. A. Synergetic Effects of Y-Zeolite and Amorphous Silica-Alumina as Main FCC Catalyst Components on Triisopropylbenzene Cracking and Coke Formation. *Fuel Process. Technol.* **2009**, *90* (2), 171–179.

(22) Qian, X. F.; Li, B.; Hu, Y. Y.; Niu, G. X.; Zhang, D. Y. H.; Che, R. C.; Tang, Y.; Su, D. S.; Asiri, A. M.; Zhao, D. Y. Exploring Meso-/Microporous Composite Molecular Sieves with Core–Shell Structures. *Chem. – A Eur. J.* **2012**, *18* (3), 931–939.

(23) Kortunov, P.; Vasenkov, S.; Kärger, J.; Valiullin, R.; Gottschalk, P.; Fé Elía, M.; Perez, M.; Stöcker, M.; Drescher, B.; McElhiney, G.; et al. The Role of Mesopores in Intracrystalline Transport in USY Zeolite: PFG NMR Diffusion Study on Various Length Scales. *J. Am. Chem. Soc.* **2005**, *127* (37), 13055–13059.

(24) Janssen, A. H.; Koster, A. J.; de Jong, K. P. On the Shape of the Mesopores in Zeolite Y: A Three-Dimensional Transmission Electron Microscopy Study Combined with Texture Analysis. *J. Phys. Chem. B* **2002**, *106* (46), 11905–11909.

(25) Milina, M.; Mitchell, S.; Cooke, D.; Crivelli, P.; Pérez-Ramírez, J. Impact of Pore Connectivity on the Design of Long-Lived Zeolite Catalysts. *Angew. Chem. Int. Ed.* **2015**, *54* (5), 1591–1594.

(26) Kärger, J.; Ruthven, D. M.; Theodorou, D. N. *Diffusion in Nanoporous Materials*; Wiley, 2012.

(27) Buurmans, I. L. C.; Ruiz-Martínez, J.; Knowles, W. V; van der Beek, D.; Bergwerff, J. A.; Vogt, E. T. C.; Weckhuysen, B. M. Catalytic Activity in Individual Cracking Catalyst Particles Imaged throughout Different Life Stages by Selective Staining. *Nat. Chem.* **2011**, *3*, 862.

(28) Kärger, J.; Valiullin, R. Mass Transfer in Mesoporous Materials: The Benefit of Microscopic Diffusion Measurement. *Chem. Soc. Rev.* **2013**, *42* (9), 4172–4197.

(29) Schneider, D.; Mehlhorn, D.; Zeigermann, P.; Kärger, J.; Valiullin, R. Transport Properties of Hierarchical Micro–Mesoporous Materials. *Chem. Soc. Rev.* **2016**, *45* (12), 3439–3467.

(30) Meunier, F. C.; Verboekend, D.; Gilson, J.; Groen, J. C.; Pérez-ramírez, J. Microporous and Mesoporous Materials Influence of Crystal Size and Probe Molecule on Diffusion in Hierarchical ZSM-5 Zeolites Prepared by Desilication. *Microporous Mesoporous Mater.* **2012**, *148* (1), 115–121.

(31) Funke, H. H.; Kovalchick, M. G.; Falconer, J. L.; Noble, R. D. Separation of Hydrocarbon Isomer Vapors with Silicalite Zeolite Membranes. *Ind. Eng. Chem. Res.* **1996**, *35* (5), 1575–1582.

(32) Bazin, P.; Alenda, A.; Thibault-Starzyk, F. Interaction of Water and Ammonium in NaHY Zeolite as Detected by Combined IR and Gravimetric Analysis (AGIR). *Dalt. Trans.* **2010**, *39* (36), 8432–8436.

(33) Bordiga, S.; Lamberti, C.; Bonino, F.; Travert, A. Probing Zeolites by Vibrational Spectroscopies. *Chem. Soc. Rev.* **2015**, *44* (14), 7262–7341.

(34) Vimont, A.; Thibault-Starzyk, F.; Daturi, M. Analysing and Understanding the Active Site by IR Spectroscopy. *Chem. Soc. Rev.* **2010**, *39* (12), 4928–4950.

(35) McCue, A. J.; Mutch, G. A.; McNab, A. I.; Campbell, S.; Anderson, J. A. Quantitative Determination of Surface Species and Adsorption Sites Using Infrared Spectroscopy. *Catal. Today* **2016**, *259*, 19–26.

(36) Kresge, C. T.; Leonowicz, M. E.; Roth, W. J.; Vartuli, J. C.; Beck, J. S. Ordered Mesoporous Molecular Sieves Synthesized by a Liquid-Crystal Template Mechanism. *Nature* **1992**, *359* (6397), 710–712.

(37) Ivanova, I. I.; Knyazeva, E. E. Micro-Mesoporous Materials Obtained by Zeolite Recrystallization: Synthesis, Characterization and Catalytic Applications. *Chem. Soc. Rev.* **2013**, *42*, 3671–3688.

(38) Peng, P.; Wang, Y.; Zhang, Z.; Qiao, K.; Liu, X.; Yan, Z.; Subhan, F.; Komarneni, S. ZSM-5-Based Mesostructures by Combined Alkali Dissolution and Re-Assembly: Process Controlling and Scale-Up. *Chem. Eng. J.* **2016**, *302*, 323–333.

(39) Suzuki, K.; Noda, T.; Katada, N.; Niwa, M. IRMS-TPD of Ammonia : Direct and Individual Measurement of Brønsted Acidity in Zeolites and Its Relationship with the Catalytic Cracking Activity. *J. Catal.* **2007**, *250*, 151–160.

(40) Konno, H.; Okamura, T.; Kawahara, T.; Nakasaka, Y.; Tago, T.; Masuda, T. Kinetics of N-Hexane Cracking over ZSM-5 Zeolites–Effect of Crystal Size on Effectiveness Factor and Catalyst Lifetime. *Chem. Eng. J.* **2012**, *207*, 490–496.

(41) Vattipalli, V.; Qi, X.; Dauenhauer, P. J.; Fan, W. Long Walks in Hierarchical Porous Materials Due to Combined Surface and Configurational Diffusion. *Chem. Mater.* **2016**, *28*, 7852–7863.

(42) Groen, J. C.; Zhu, W.; Brouwer, S.; Huynink, S. J.; Kapteijn, F.; Moulijn, J. A.; Pérez-Ramírez, J. Direct Demonstration of Enhanced Diffusion in Mesoporous ZSM-5 Zeolite Obtained via Controlled Desilication. *J. Am. Chem. Soc.* **2006**, *129* (2), 355–360.

(43) Zecchina, A.; Bordiga, S.; Spoto, G.; Scarano, D.; Petrini, G.; Leofanti, G.; Padovan, M.; Areàn, C. O. Low-Temperature Fourier-Transform Infrared Investigation of the Interaction of CO with Nanosized ZSM5 and Silicalite. *J. Chem. Soc. Faraday Trans.* **1992**, *88* (19), 2959–2969.

(44) Cerqueira, H. S.; Caeiro, G.; Costa, L.; Ramôa Ribeiro, F. Deactivation of FCC Catalysts. *J. Mol. Catal. A Chem.* **2008**, *292* (1), 1–13.

(45) Vogt, E. T. C.; Weckhuysen, B. M. Fluid Catalytic Cracking: Recent Developments on the Grand Old Lady of Zeolite Catalysis. *Chem. Soc. Rev.* **2015**, *44* (20), 7342–7370.